Article ID: 1006-8775(2020) 02-0176-12

Operational Evaluation of the Quantitative Precipitation Estimation by a CINRAD–SA Dual Polarization Radar System

CHEN Chao (陈 超) [1, 2], LIU Li-ping (刘黎平) [2], HU Sheng (胡 胜) [1], WU Zhi-fang (伍志方) [1], WU Chong (吴 翀) [2], ZHANG Yang (张 扬) [2]

(1. Guangdong Meteorological Observatory, Guangzhou 510641 China; 2. State Key Laboratory of Severe Weather, Chinese Academy of Meteorological Sciences, Beijing 100081 China)

Abstract: In this paper, a quantitative precipitation estimation based on the hydrometeor classification (HCA-QPE) algorithm was proposed for the first operational S band dual-polarization radar upgraded from the CINRAD/SA radar of China. The HCA-QPE algorithm, localized Colorado State University-Hydrometeor Identification of Rainfall (CSU-HIDRO) algorithm, the Joint Polarization Experiment (JPOLE) algorithm, and the dynamic *Z-R* relationships based on variational correction QPE (DRVC-QPE) algorithm were evaluated with the rainfall events from March 1 to October 30, 2017 in Guangdong Province. The results indicated that even though the HCA-QPE algorithm did not use the observed rainfall data for correction, its estimation accuracy was better than that of the DRVC-QPE algorithm when the rainfall rate was greater than 5 mm h^{-1}; and the stronger the rainfall intensity, the greater the QPE improvement. Besides, the HCA-QPE algorithm worked better than the localized CSU-HIDRO and JPOLE algorithms. This study preliminarily evaluated the improved accuracy of QPE by a dual-polarization radar system modified from CINRAD-SA radar.

Key words: quantitative precipitation estimation; operational QPE evaluation with dual-polarization radar; optimization algorithm; dual-polarization radar; hydrometeor classification; dynamic *Z-R* relations algorithm

CLC number: P412.25 **Document code:** A

https://doi.org/10.46267/j.1006-8775.2020.016

1 INTRODUCTION

Improving the accuracy of quantitative precipitation estimation (QPE) is important for the early warning of heavy rainfall. A dual-polarization radar can transmit and receive horizontally and vertically polarized radiations simultaneously, which ensures that we can obtain not only the radar reflectivity Z, but also the differential reflectivity (Z_{DR}) and the specific differential propagation phase (K_{DP}). These polarization parameters provide considerable information with respect to the shape and phase of hydrometeor particles. Plenty studies have shown that there will be an improvement in rainfall estimation if these parameters are used, and polarimetric rainfall estimation techniques are more robust with respect to drop size distribution (DSD) variations than the conventional *Z-R* relationship (Chandrasekar et al. [1]; Gorgucci et al. [2]; Ryzhkov et al. [3]; Cifelli et al. [4]).

QPE with a dual-polarization radar mainly includes four basic estimators, i.e., $R(Z_H)$, $R(Z_H, Z_{DR})$, $R(K_{DP})$, and $R(K_{DP}, Z_{DR})$. These estimators utilize Z, Z_{DR}, and K_{DP} in different combinations (Ryzhkov et al. [3, 5]; Chen et al. [6]). Because different estimators have different estimation accuracies for different rainfall rates or hydrometeor phases (Chandrasekar et al. [1, 7]; Ryzhkov et al. [5]; Zrnić and Ryzhkov [8]), a majority of studies currently seek to optimize estimates through combining these estimators (Ryzhkov et al. [3]; Pepler [9]; Chen et al. [6]). In this paper, we call these approaches as optimization algorithms.

Previous studies show that these optimized algorithms work very well in different countries or regions (Ryzhkov et al. [3]; Pepler et al. [9]). For example, the JPOLE optimized combination algorithm proposed by Ryzhkov et al. [3] used the $R(Z_H)$ result as a criterion for differentiating between three

Received 2019-03-01; **Revised** 2020-02-15; **Received** 2020-05-15

Funding: National Key Research and Development Program of China (2017YFC1404700, 2018YFC1506905); Open Research Program of the State Key Laboratory of Severe Weather (2018LASW-B09, 2018LASW-B08); Science and Technology Planning Project of Guangdong Province, China (2019B020208016, 2018B020207012, 2017B020244002); National Natural Science Foundation of China (41375038); Special Scientific Research Fund of Meteorological Public Welfare Profession of China(GHY201506006); 2017-2019 Meteorological Forecasting Key Technology Development Special Grant (YBGJXM(2017)02-05); Guangdong Science & Technology Plan Project (2015A020217008); Zhejiang Province Major Science and Technology Special Project (2017C03035); Scientific and Technological Research Projects of Guangdong Meteorological Service(GRMC2018M10); Natural Science Foundation of Guangdong Province (2018A030313218)

Biography: CHEN Chao, primarily undertaking research on rainstorm and atmospheric measurement and remote sensing.

Corresponding author: LIU Li-ping, e-mail: liulp@cma.gov.cn

levels of rainfall rates: $R(Z_H) \leqslant 6$ mm h^{-1}, $6 \leqslant R(Z_H) \leqslant 50$ mm h^{-1}, and $R(Z_H) > 50$ mm h^{-1}. In addition, different QPE estimators were selected to calculate rainfall rates. Pepler et al.[9] used reflectivity factor as a criterion to select estimators and achieved good results. These optimized algorithms used $R(Z_H)$ or the reflectivity factor to determine which method to employ for a given set of polarimetric observables. But the validated area of these optimized algorithms is below the melting layer where the contamination from mixed-phase and frozen hydrometeors is minimal. In 2011, Colorado State University (CSU) proposed the CSU-HIDRO algorithm (Cifelli et al.[4]), which used the classification of hydrometeor based on fuzzy logic identification (Park et al.[10]) to differentiate the hydrometeor particles in liquid, mixed-phases, and ice. They were further combined with various polarization parameters (Z, Z_{DR}, and K_{DP}) thresholds to select different QPE estimators. Before the CSU-HIDRO algorithm, Giangrande et al.[11] suggested the EC method for rainfall estimation that capitalizes on the results of polarimetric echo classification. These studies indicated that the radar QPE optimized combination algorithm based on hydrometeor classification performed better than other optimization algorithms (Giangrande et al.[11]; Cifelli et al.[4]).

In Guangdong, there are frequent occurrences of non-liquid hydrometeors (hail) during the process of strong convection in the annually first rainy season (April to June), and multiple radar networking is needed. Therefore, it is necessary to identify such non-liquid hydrometeors before QPE. Through modification based on the statistical analysis of polarimetric variables, a localized hydrometeor classification algorithm (HCA) that is suited for southern China is obtained (Wu et al.[12]). In this study, we divide the classification results into liquid, mixed-phases, and ice. In addition, because DSDs and rainfall error characteristics vary considerably among studies and locations, the localized estimators are fitted based on the DSD data observed in Guangdong. Subsequently, we combined the polorimetric parameters, and proposed a QPE algorithm based on the hydrometeor-classification (HCA-QPE).

Currently, the QPE algorithm used in Guangdong is the dynamic Z–R relationships algorithm based on variation correction (Wang et al.[13]) (hereafter referred to as DRVC-QPE). The main feature of this algorithm is that Z–R relationships were fitted by radar measured Z and rainfall rate by rain gauges every 60 minutes. The CSU-HIDRO and JPOLE (Ryzhkov et al.[3]) algorithms that were used in this study for a comparison with the proposed HCA-QPE algorithm did not involve correction with the measured rainfall data from rain gauges. The CSU-HIDRO and JPOLE algorithms had been reported to show good performance in applications of other regions. However, in Guangdong, the radar hardware level and DSD observed under the local climatic background are quite different from those of other regions. Therefore, the feasibility studies of the application of these two algorithms in Guangdong would require a localization approach.

So far, 11 S-band dual-polarization radars have been set up in Guangdong Province, including the Guangzhou S-band dual-polarization radar (hereinafter referred to as the Guangzhou radar), which is the first dual-polarization radar in China upgraded from the operational CINRAD/SA weather radar. By 2020, more than 100 dual-polarization radars will be built or upgraded in China. In previous studies in China, QPE with dual-polarization radars were mostly performed to estimate the QPE only for research purposes (Wei et al.[14]), and studies on operational radars were limited to a single method for individual events (Wang et al.[15]). The operational QPE by the newly-built S-band dual-polarization radar was not evaluated. Therefore, it is highly valuable to quantitatively evaluate the actual influence of the dual-polarization radar on QPE with immediate attention.

In this paper, the new optimized algorithm (HCA-QPE), the localized CSU-HIDRO and JPOLE algorithms, and the DRVC-QPE algorithm operating in Guangdong Province were applied to estimate the rainfall of Guangzhou radar continuous observation data from March 1 to October 30, 2017. The error characteristics of these algorithms were compared, and the improvement of the operational QPE by the dual-polarization radar were analyzed.

2 DATA

2.1 *Data resource*

The Guangzhou radar became operational in May 2016. The radar operates in the conventional VCP21 volume-scan mode and completes a volume scan using nine specific elevation angles (0.5°, 1.5°, 2.4°, 3.3°, 4.3°, 6.0°, 9.9°, 14.6°, and 19.5°) in 6 min. The parameters of the radar are presented in Table 1.

From March 1 to October 30, 2017, the Guangzhou Radar observed 67 rainfall events with the rain gauges in the 100 - range of the Guangzhou radar observed precipitation, such as squall lines and typhoons. The maximum rainfall rate was 183.4 mm h^{-1}. In total, there are 48, 271 records of hourly rainfall rates that were greater than 1-mm h^{-1}, 22,189 records of 1–5-mm h^{-1}, 13, 171 records of 5–10 - mm h^{-1}, 8,839 records of 10–20 - mm h^{-1}, 3,854 records of 20–50-mm h^{-1}, and 274 records of more than 50 - mm h^{-1}. Table 2 (see the appendix) presents the duration and types of rainfall events with a duration more than 5 hours.

In this study, the DSD data from 8 OTT disdrometers and 3 Metstar (Beijing Metstar Radar Co., Ltd.) disdrometers in Guangdong in 2014, 2016, and 2017 were used to fit the QPE estimators. After the quality control procedure (Zhang et al.[16]), there were 17, 326 1-min valid DSD samples. The spatial

Table 1. The main technical parameters of the Guangzhou dual-polarization radar.

Variable	Parameter
Antenna diameter	8.5 m
Antenna gain	≥44 dB
Bean width	0.95°
Frequency	2885 MHz
Peak power	≥325 kW
Pulse width	1.57 us, 4.7 us
Pulse repetition frequency	322 Hz−1304 Hz
Work model	Simultaneously transmit and receive
Minimum detectable power	≤−109 dBm (1.57 us) ≤−114 dBm (4.7 us)
Noise	≤4 dB
Dynamic range	≥85 dB
Range resolution	250 m/1000 m
Observation accuracy	Z≤ 1dB Z_{DR} ≤ 0.2dB Φ_{DP} ≤ 2° K_{DP} ≤ 0.2° km^{-1} $\rho_{HV}(0)$ ≤ 0.001

distribution of the disdrometers is depicted in Fig. 1. The hourly rainfall data measured by more than 1600 rain gauges in Guangdong Province were used to evaluate QPE.

2.2 *Data preprocessing and quality control*

After Guangzhou radar construction, a series of tests, such as built-in testing, sun-calibration, and vertical pointed calibration were conducted by the Meteorological Observation Center, China Meteorological Administration. And the result of the test indicated that Z_{DR} accuracy is better than 0.2 dB (Chen et al. [17]). The quality control of the radar data was conducted prior to performing the radar QPE as follows:

(1) noise correction for $\rho_{HV}(0)$ and Z_{DR} based on the assumption that the horizontal and vertical channel noise levels of the dual-polarization radar are consistent (Liu et al. [18]);

(2) all data with $\rho_{HV}(0) < 0.7$, $Z > 40$ dB and absolute value of radial velocity less 0.5 m s^{-1} were removed to exclude non meteorological echoes;

(3) all negative values of Z_H , Z_{DR} and K_{DP} were removed, and the values of Z_H , and Z_{DR} were smoothed over 5 range gates to remove noisiness in the raw data, particularly for Z_{DR};

(4) in this study, K_{DP} is estimated by Φ_{DP} using the algorithm like the one in Wang et al. [19] after 5-gate smoothing filter was applied to the basic Φ_{DP} data in each ray.

The CAPPI reflectivity at a 3-km altitude with a horizontal resolution of 0.01° × 0.01° is used in DRVC-QPE, while the remaining radar QPE algorithms use hybrid scanning. When the scanning data at elevation 0.5° is blocked, data with higher layer will be used, and so on.

Additionally, the processing of DSD data in this study refers to the method reported by Zhang et al. [20]. The assessment requires consecutive observation records by the rain gauge for 24 hours; otherwise, the automatic station would be considered to be unreliable and would be rejected.

3 QPE ALGORITHMS

The QPE that uses dual-polarization radar data mainly includes four basic estimator, including $R(Z_H)$, $R(Z_H, Z_{DR})$, $R(K_{DP})$, and $R(K_{DP}, Z_{DR})$. The estimators are as follows:

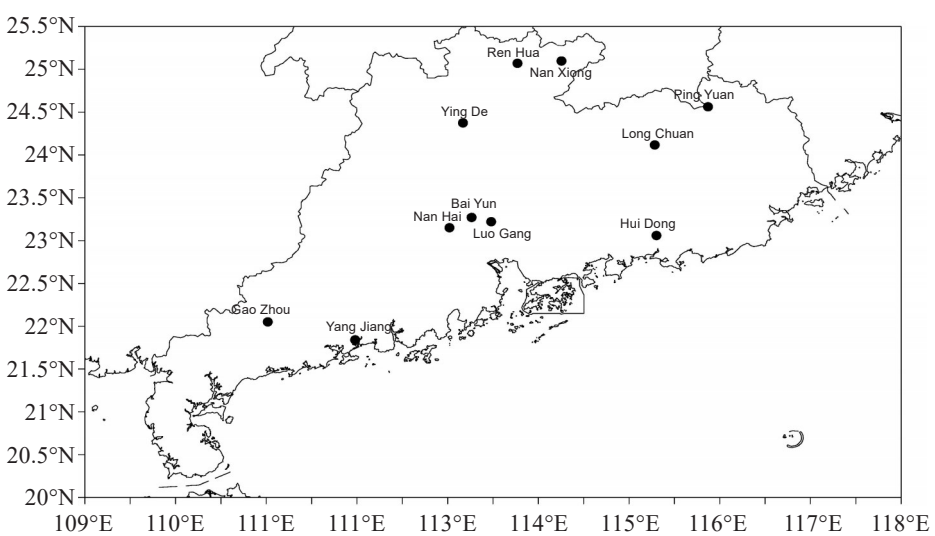

Figure 1. Distribution of disdrometers in Guangdong Province.

$$R(Z_H) = a_1 \times Z_H^{b_1}, \quad (1)$$

$$R(K_{DP}) = a_2 \times K_{DP}^{b_2}, \quad (2)$$

$$R(Z_H, Z_{DR}) = a_3 \times Z_H^{b_3} \times 10^{c_3 \times Z_{DR}}, \quad (3)$$

$$R(K_{DP}, Z_{DR}) = a_4 \times K_{DP}^{b_4} \times 10^{c_4 \times Z_{DR}}, \quad (4)$$

where a, b, and c are the coefficients; R is the rainfall rate in mm h^{-1}; Z_H is the reflectivity factor in mm^6 m^{-3}.

In the case of light rain, the polarization parameters of Z_{DR} and K_{DP} are observed to be relatively small with a few obvious fluctuations that can be attributed to noise (Chen et al. [17]); therefore, $R(Z_H, Z_{DR})$, $R(K_{DP})$, and $R(K_{DP}, Z_{DR})$ exhibit no advantages over the $R(Z_H)$ method in this case (Chandrasekar et al. [1]). As the rainfall rate increases, the deformation of raindrops becomes significantly reduced. Z_{DR} is the polarization parameter that characterizes this deformation information. Hence, the $R(Z_H, Z_{DR})$ and $R(K_{DP}, Z_{DR})$ based on Z_{DR} exhibit significant advantages, and Ryzhkov et al. [5] depicted that $R(K_{DP}, Z_{DR})$ resulted in considerably accurate predictions with respect to precipitation in case of medium to high intensities. With a further increase in rainfall intensity, especially when the precipitation contains non-liquid forms, $R(K_{DP})$ provides distinctively accurate estimations because the parameter that characterizes the phase variability of the radar beam after it passes through the precipitation particles, K_{DP}, is considerably resilient to the attenuation and particle phase effects (Chandrasekar et al. [1]).

Currently, the dual-polarization radar QPE is usually performed by combining these estimators, which can be referred to as the optimization algorithm. The localized JPOLE algorithm (Ryzhkov et al. [3]), the localized CSU-HIDRO (Cifelli et al. [4]), and the HCA-QPE algorithm proposed in this study are all optimization algorithms.

3.1 *HCA-QPE algorithm*

To develop an optimization algorithm, it is first necessary to localize the estimators. Based on the DSD data observed in Guangdong, the estimator coefficients that are suitable for the annually first rainy season and annually second rainy season (July to September) in Guangdong were fitted by using the piecewise fitting method (Zhang et al. [16]). The results are listed in Tables 3 and 4. In this study, the HCA suggested by Wu et al. [12] was used to classify the hydrometeors, and we divided the classification results into liquid, mixed-phases, and ice, and we subsequently combined the polarimetric parameters to guide the choice of estimators. The HCA-QPE algorithm flowchart is depicted in Fig. 2, where NaN represents an invalid value. An analysis of the polarization radar data indicates that noise can easily affect the Z_{DR} and K_{DP} when the SNR is < 20 dB, leading to large spatiotemporal variations (Chen et al. [17]). Therefore, the $R_1(Z_H)$ used for light rain (Zhang et al. [20]) is used to perform the estimation under these SNR conditions because the Z_{DR} and K_{DP} are not appropriate for light rain estimation. In this study, the threshold of Z_H is the same with CSU-HIDRO algorithm (Cifelli et al. [4]), and after a large number of experiments, the threshold of Z_{DR} and K_{DP} are concluded (Fig. 2).

Table 3. The QPE estimator coefficients of the annually first rainly season.

Estimators	Coefficient a	Coefficient b	Coefficient c
$R_1(Z_H)$	0.0082	0.749	
$R_2(Z_H)$	0.0154	0.7681	
$R_1(K_{DP})$	30.30	0.9298	
$R_2(K_{DP})$	33.6142	0.8332	
$R(Z_H, Z_{DR})$	0.0084	0.9284	−0.4055
$R(K_{DP}, Z_{DR})$	51.16	0.9311	−0.0852

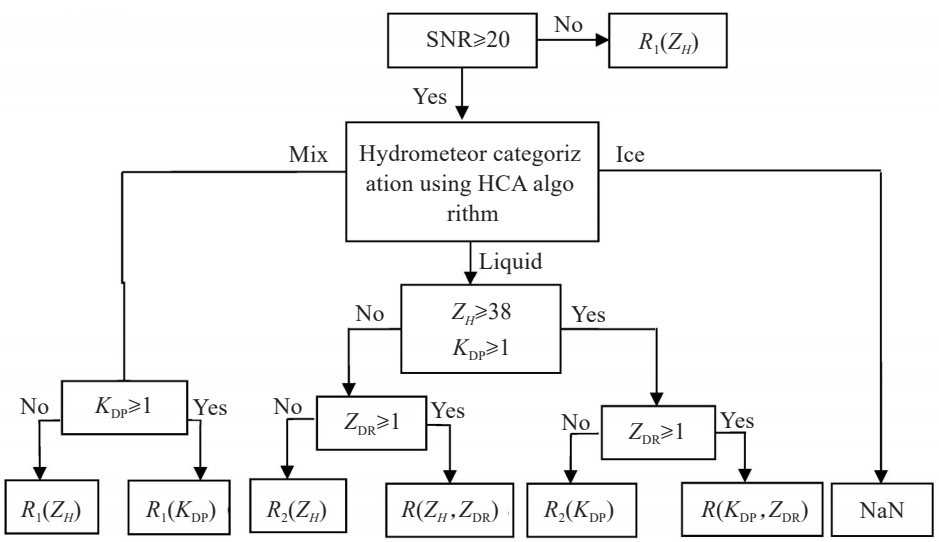

Figure 2. Flowchart of the HCA-QPE algorithm.

Table 4. The QPE estimator coefficients of the annually second rainy season.

Estimators	Coefficient a	Coefficient b	Coefficient c
$R_1(Z_H)$	0.03966	0.6246	
$R_2(Z_H)$	0.0135	0.7923	
$R_1(K_{DP})$	33.82	0.8678	
$R_2(K_{DP})$	46.29	0.8941	
$R(Z_H, Z_{DR})$	0.00892	0.9078	−0.3573
$R(K_{DP}, Z_{DR})$	60.5	0.9638	−0.124

3.2 *Localized CSU-HIDRO and JPOLE algorithms*

The CSU-HIDRO algorithm has been described in Cifelli et al. [4]. In this paper, we used the HCA suggested by Wu et al. [12] as the guide of the choice of the estimators. And the coefficients of each estimator were refitted using the DSD data recorded in Guangdong. The results are listed in Tables 5 and 6.

Table 5. The QPE estimator coefficients of the annually first rainy season.

Estimators	Coefficient a	Coefficient b	Coefficient c
$R(Z_H)$	0.0082	0.749	
$R(K_{DP})$	32.2886	0.8991	
$R(Z_H, Z_{DR})$	0.0047	0.9624	−0.3574
$R(K_{DP}, Z_{DR})$	52.656	0.9721	−0.0996

Table 6. The QPE estimator coefficients of the annually second rainy season.

Estimators	Coefficient a	Coefficient b	Coefficient c
$R(Z_H)$	0.03966	0.6246	
$R(K_{DP})$	35.69	0.8376	
$R(Z_H, Z_{DR})$	0.01014	0.9029	−0.3739
$R(K_{DP}, Z_{DR})$	60.8	0.9516	−0.1241

According to the JPOLE (Ryzhkov et al. [3]) optimization algorithm, the choice between various estimators is determined solely by the rainfall rate computed from $R(Z_H)$ relation. In this paper, the coefficients of each estimators were refitted using the DSD data recorded in Guangdong. The results are listed in Tables 5 and 6. Because the JPOLE algorithm uses rainfall rate as a threshold to select different QPE estimators, $R(K_{DP})$, $R(Z_H, Z_{DR})$, and $R(K_{DP}, Z_{DR})$ may provide invalid or large false values when Z_{DR} or K_{DP} is either small and unstable or negative. To avoid this, $R(Z_H)$ is used as the final QPE result under the aforementioned conditions.

3.3 *Operational QPE algorithm in Guangdong Province (dynamic Z-R relations based on variational correction QPE algorithm (DRVC-QPE))*

Because of the variation in the DSD of precipitation and the error of reflectivity factor, it is impossible to obtain a stable Z–R relation. Currently, the dynamic Z–R relations algorithm is used for the radar QPE in China (Wang et al. [13]; Chen et al. [21]). To further improve the accuracy of radar QPE, the variational correction method (Zhang et al. [22]) is applied to the operational dynamic Z–R relations algorithm in Guangdong Province.

In this paper, a total of 810 rain gauges that were randomly chosen from half of the gauges in the coverage of the Guangzhou radar volume scan were used. Because this is a QPE algorithm for operational services in Guangdong Province, the parameters a and b of $Z = a \times R^b$ were time-averaged value before the period considered in this study, i. e., before 00: 00 March 1, 2017. The starting values were 16 and 2.45. Furthermore, the Z–R coefficients were refitted every 60 minutes and were used for the subsequent 6-min radar QPE. From March 1 to October 30, 2017, the value of a fluctuated between 16 and 250, and the value of b fluctuated between 1.2 and 2.85.

3.4 *Evaluation methods*

The radar QPE results were evaluated using the mean absolute error (AE), the average relative error (RE), the ratio deviation (BIAS) and the root mean square error (RMSE). These parameters are calculated as:

$$\mathrm{AE} = \frac{1}{n}\sum_{i=1}^{n}\left| G_i - R_i \right|, \tag{5}$$

$$\mathrm{RE} = \frac{\frac{1}{n}\sum_{i=1}^{n}|G_i - R_i|}{\frac{1}{n}\sum_{i=1}^{n} G_i}, \tag{6}$$

$$\mathrm{BIAS} = \frac{\frac{1}{n}\sum_{i=1}^{n} R_i}{\frac{1}{n}\sum_{i=1}^{n} G_i}, \tag{7}$$

$$\mathrm{RMSE} = \sqrt{\frac{1}{n}\sum_{i=1}^{n} (G_i - R_i)^2}, \tag{8}$$

where G_i denotes the 1-h observed rainfall of the i-th rain gauge sample in the evaluation data set, R_i denotes the 1-h estimated rainfall with radar, and n denotes the number of effective QPE-rain gauge pairs.

Because the DRVC-QPE algorithm requires rain gauges to correct retrieved rainfall rate, all of rain gauges are divided nto two group; one is for correction and the other is for evaluation. Because of the $R(Z_H)$, HCA-QPE, CSU-HIDRO, and JPOLE algorithms in this study did not use the rain gauges rainfall for real-time

correction, the evaluation station can simply be selected from within a given distance range.

4 RESULT ANALYSIS

The QPEs with HCA-QPE, CSU-HIDRO, JPOLE, and DRVD-QPE algorithms were performed for rainfall events from March 1 to October 30, 2017 shown in Table 2. The dual-polarization radar QPE capability is evaluated in different rainfall levels and range from radar site.

4.1 *Error analysis of different precipitation intensities*

In this analysis, the hourly rainfall measured by the rain gauges can be divided into 5 levels, including 1–5mm, 5–10mm, 10–20mm, 20–50mm, and 50mm and above. Table 7 presents the results using the HCA-QPE, CSU-HIDRO, JPOLE, DRVC-QPE, and $R(Z_H)$ algorithms for five rain fall levels.

Previous studies have demonstrated that the fixed Z–R relationship $R(Z_H)$ underestimated all types of precipitation (Gou et al.[23]). Although the $R(Z_H)$ is fitted from local DSDs data in Guangdong, the QPE is also underestimated. It can be observed from Table 7 that the maximum BIAS for $R(Z_H)$ is 0.87. The BIAS gradually declined with the rainfall rate. For a rainfall rate >50mm h^{-1}, the BIAS is only 0.49. The DRVC-QPE algorithm considerably improved the underestimation due to the corrections by rain gauge data. The BIAS increased by 28.2% in total while the root-mean-square error (RMSE) was reduced by 22.4% (1.79 mm). However, for the 1−5mm h^{-1} rainfall rate, the DRVC-QPE is overestimated (BIAS is 1.12) with large values of RE and RMSE.

Table 7. The QPE evaluation results from March 1 to October 30, 2017.

Precipitation Estimation Algorithm	Evaluation Method	Hourly Rainfall (mm)					Average
		1–5	5–10	10–20	20–50	⩾50	
HCA-QPE	RE (%)	65.43	38.07	32.07	26.93	24.64	47.99
	AE (mm)	1.58	2.69	4.45	7.53	15.87	3.19
	RMSE (mm)	2.82	3.52	5.66	9.39	19.0	5.19
	BIAS	1.35	0.96	0.88	0.83	0.74	0.93
CSU-HIDRO	RE (%)	53.78	45.75	39.44	35.32	36.94	49.92
	AE (mm)	1.47	3.26	5.48	10.12	33.35	3.94
	RMSE (mm)	2.45	4.12	6.54	11.87	26.3	6.28
	BIAS	0.87	0.73	0.7	0.69	0.64	0.71
JPOLE	RE (%)	52.89	41.82	38.88	35.73	34.29	48.85
	AE (mm)	1.4	2.91	6.53	10.26	24.32	3.83
	RMSE (mm)	2.39	3.73	7.3	12.2	31.74	6.18
	BIAS	1.02	0.78	0.71	0.69	0.67	0.75
DRVC-QPE	RE (%)	56.45	46.28	40.96	41.17	48.56	50.15
	AE (mm)	1.31	3.3	5.76	11.93	30.34	3.31
	RMSE (mm)	2.71	4.28	7.2	14.32	34.2	6.22
	BIAS	1.12	0.84	0.71	0.64	0.54	0.78
$R(Z_H)$	RE (%)	47.12	54.73	53.85	52.8	57.5	50.96
	AE (mm)	1.4	3.91	7.53	15.28	36.36	5.03
	RMSE (mm)	1.93	4.32	8.19	16.62	37.94	8.01
	BIAS	0.77	0.69	0.6	0.53	0.49	0.56

Despite the fact that the HCA-QPE algorithm proposed in this study did not use the rain gauges data to correct the QPE results, the RE decreased by 4.3% on average, the AE reduced by 3.6% (0.12 mm) on average, and the RMSE declined 16.6% (1.03 mm) on average, whereas BIAS increased by 16.1% on average as compared with those obtained using the DRVC-QPE algorithm. However, the HCA-QPE algorithm shows a larger error as compared with that showed by the DRVC-QPE algorithm when the rainfall rate was less than 5mm h^{-1}, which was mainly due to overestimation (BIAS being 1.35). When the rainfall rate is more than 5mm h^{-1}, the error of the HCA-QPE algorithm is evidently better than that of the DRVC-QPE algorithm. As the precipitation intensified, the accuracy improved even more. At a strong rainfall rate (over 20mm h^{-1}), HCA-QPE has its RE, AE, and RMSE reduced by 34.5%, 36.9% (4.4 mm), 34.3% (4.93 mm), and BIAS increased by 29.7% as compared to that of the DRVC-QPE algorithm.

The localized CSU-HIDRO and JPOLE algorithms, in the absence of the corrections by measured rainfall data, still performed better than the DRVC-QPE algorithm when rainfall rate is more than 5mm h^{-1};

however, the rainfall rate of the localized CSU-HIDRO and JPOLE algorithms are still underestimated. The HCA-QPE algorithm proposed in this study showed the least error as compared with that by other algorithms for rainfall rates more than 5mm h^{-1}; furthermore, the higher the rainfall rate, the better the performance. Additionally, the HCA-QPE algorithm considerably improved the underestimation that was observed in other algorithms.

4.2 *Error variation with distances*

The U.S. National Weather Service (NWS) requires its S-band dual-polarization radar QPE to cover a region of 230km around the radar (Ryzhkov et al.[24]). Although we did not explicitly regulate the coverage distance, the CINRAD-SA radar products generally cover 230km for the networking between multiple radar products.

Because the CINRAD-SA dual polarization radars show a minimum scan elevation angle of 0.5° , the vertical height increases as the horizontal distance from the radar increases. Due to the increase in precipitation or evaporation, the movement of airflow, the phase change of particles, and so on, the radar observation will be altered in the vertical direction. This shift will increase with horizontal distance from the radar and with vertical distance from the ground (Shi et al. [25]).

In the melting layer, the reflectivity factor, may be 5-10dB higher inside the bright-band due to melting, collision, and slow falling speed of the snowflakes (Dai et al. [26]). Majority of the hydrometeor above the melting layer would be dry snowflakes and ice crystals with weak backscattering, which causes a decrease in the reflectivity factor and the differential reflectivity. Especially in the heights above the melting layer, the radar SNR is observed to be generally small. All the aforementioned reasons will cause the QPE results to alter with distance.

To analyze the variation characteristics of error with distance in the HCA-QPE, CSU-HIDRO, and JPOLE algorithms, this study categorized the automatic stations in the radar coverage into 9 groups at a 25-km interval with the furthest being 225km. Radar QPE was conducted for various types of precipitation from March 1 to October 30, 2017 at each distance range. BIAS and RMSE were further calculated over each distance range. Fig. 3 depicts the variation of BIAS and RMSE along the distance ranges of the three optimization algorithms.

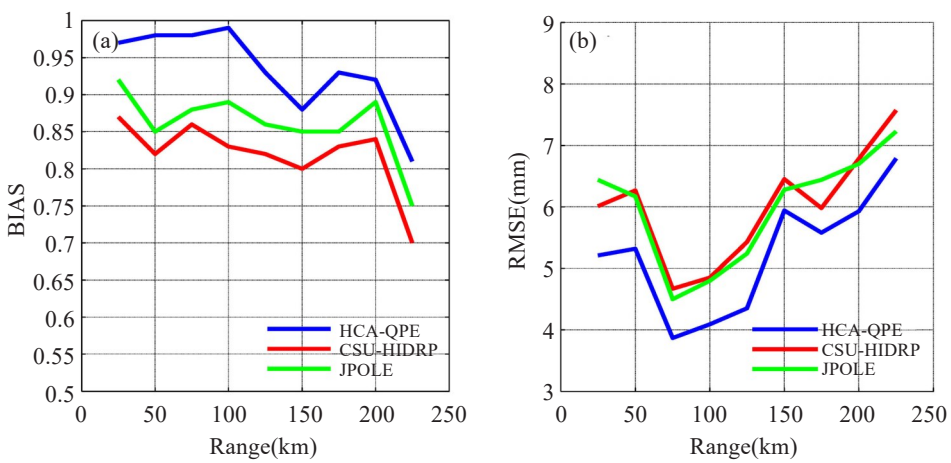

Figure 3. BIAS (a) and RMSE (b) of the three optimization algorithms with range.

The observed facts from the sounding data of 2017 (59280) indicate that the height of the 0 °C-layer during the rainy seasons in Guangdong is 3–5.5km. Based on the assumption of the standard atmosphere, the calculated horizontal distance range corresponding to the 0 ° C-layer at an elevation angle of 0.5° should be approximately 160-236km. By considering its thickness (Gatlin et al. [27]; Emory et al. [28]), the melting layer may have an impact at a horizontal distance of ⩾125km.

As depicted in Fig. 3, the radar QPE estimation results of the three optimization algorithms are smaller than the actual results (BIAS less than 1) in the range of 0–225km. The HCA-QPE algorithm is better than the other two optimization algorithms (minimum RMSE) across all the distance ranges. The three optimization algorithms perform an even better estimation in the range of 50–125km than in other ranges. That is because the influence of the grounding and melting layers on the echo is small and the QPE results are mainly affected by the distribution of raindrops and hail.

As the horizontal distance extends to approximately 125km, the radar QPE results begin to be affected by the melting layer. Based on the results of this study, the three radar QPE optimization algorithms did not show a consistent increase in and above the melting layer. There is a certain fluctuation from 125km to 200km. Beyond 200km, the altitude is close to the top of the melting layer and the majority of the hydrometeors above the melting layer comprises dry snowflakes and ice crystals with a weak backscattering effect. This would induce a decrease in the reflectivity and the differential reflectivity. Because the specific differential propagation phase reduces while passing through the non-liquid region, the estimation results tend to be small. In any

case, it can clearly be observed from Fig. 3b that the RMSE of the three optimization algorithms increases rapidly while reaching the melting layer or beyond, indicating that the existence of the melting layer reduces the accuracy of QPE.

5 CASE STUDY

During May 14–16, 2017, Guangdong experienced a large-scale heavy rain because of the influence of the westerly trough and the lower shear line. The precipitation was concentrated in the Pearl River Delta, where the hourly rainfall was mostly distributed in a strip shape. The precipitation shows the characteristics of large area and strong intensity. Short-term strong precipitation was recorded by multiple stations within the 20–100km range of the Guangzhou radar, and the maximum hourly rainfall rate became 119.1mm h^{-1}.

Based on the error results, all the three optimization algorithms presented better evaluation results as compared with those presented by the DRVC-QPE and $R(Z_H)$ algorithms when the rain rate became > 10mm h^{-1}in this precipitation event. Among the three optimal combination algorithms, HCA-QPE was the best algorithm with an average RE of 40.17%, AE of 2.68 mm, RMSE of 4.75 mm, and BIAS of 0.84.

From the perspective of spatial distribution, there were two rainfall belts in the central and southern Guangdong at 01: 00 on May 16, 2017. All the algorithms showed an ability to describe the main features of precipitation in spatial distribution. The DRVC-QPE algorithm requires segregation of gauges for corrections and gauges for evaluation, and the QPE value of the gauges participating in the correction of the service is the same as the measured rainfall value from the rainfall gauges. Therefore, this algorithm showed the best correspondence in precipitation maxima and most of the precipitation spatial distribution (Fig. 4c) with the measured rainfall from the rain gauges (Fig. 4a). The other algorithms, as can be observed, showed smaller estimation than that showed by the measured rainfall in the strong precipitation area. Apart from the DRVC-QPE algorithm, the HCA-QPE algorithm is the most ideal for the spatial distribution of precipitation (Fig. 4f). In addition, this study also provides an hourly precipitation distribution map for typhoon landing (Fig. 5). As can be observed from the figure, the precipitation showed obvious regional characteristics, and the results of each radar QPE algorithm can also reflect the basic distribution characteristics of precipitation. Except for the DRVC-QPE algorithm, the results of all the other algorithms are weaker than the measured rainfall.

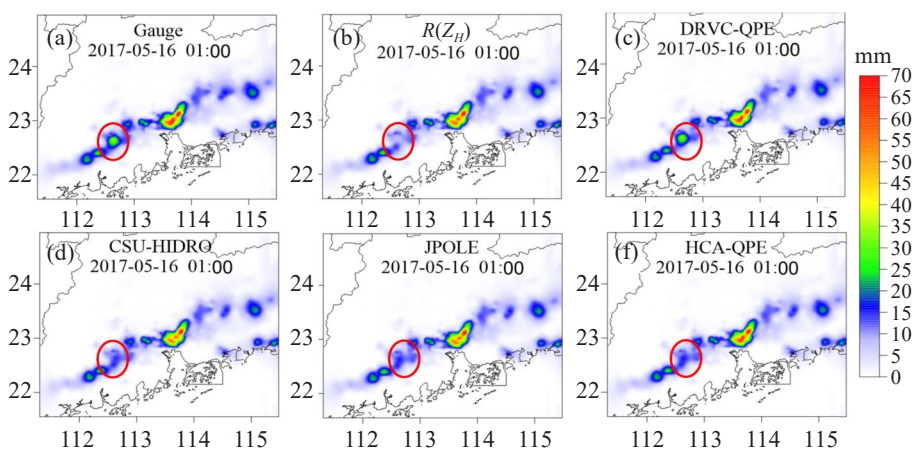

Figure 4. Hourly rainfall of the gauge and radar QPE by various algorithms at 01:00 May 16, 2017.

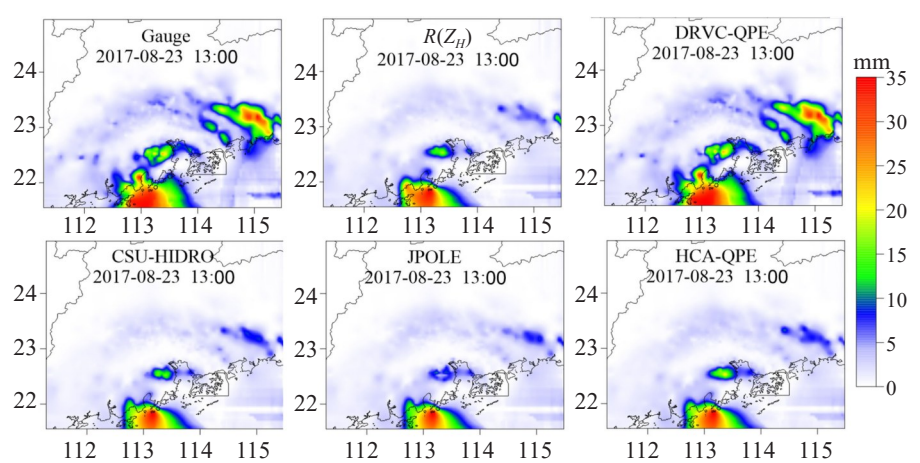

Figure 5. Hourly rainfall of the gauge and radar QPE by various algorithms at 13:00 August 23, 2017.

As revealed from Fig. 6, the error of $R(Z_H)$ is mainly caused by the underestimation improved by the DRVC-QPE algorithm at all levels of rainfall rate, but there are still a good number of stations that could not be well corrected. It can also be observed that the common feature of the algorithms is the underestimation as the rainfall rate increases, which is consistent with the BIAS analysis in Table 7. And the HCA-QPE algorithm has considerably eliminated underestimation; however, the error remains in different rainfall rates.

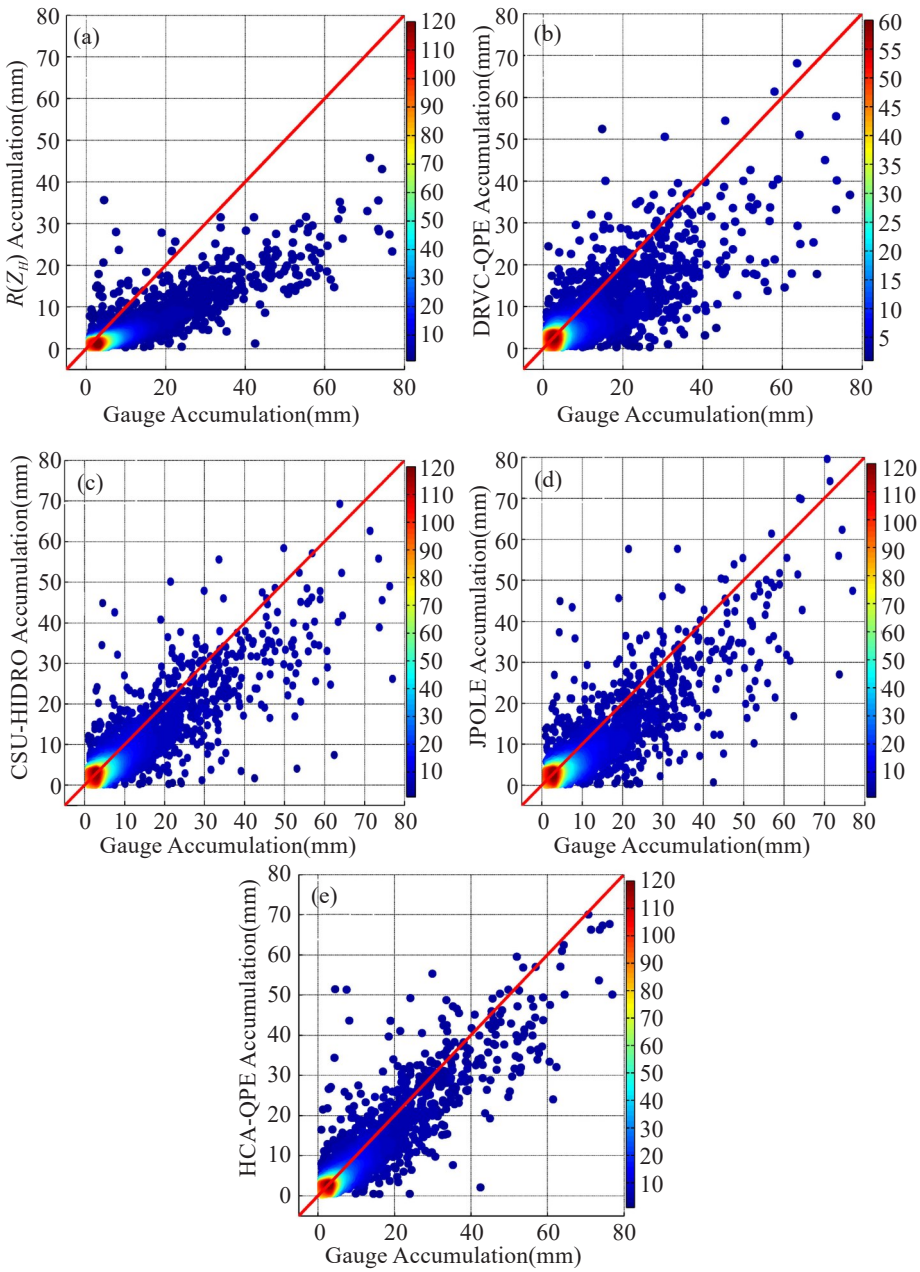

Figure 6. Probability density plots of hourly radar-gauge rainfall accumulation on 08:00 May 14 to 08:00 May 16, 2017. (a) $R(Z_H)$, (b) DRVC-QPE, (c) CSU-HIDRO, (d) JPOLE, and (e) HCA-QPE.

6 CONCLUSION

This study proposed the HCA-QPE for Guangdong region. Based on the quality control and data processing of observation data, the HCA-QPE algorithm, the localized CSU-HIDRO and JPOLE algorithms, and the DRVC-QPE algorithm currently operating in Guangdong were applied to rainfall estimation. The results were analyzed in different rainfall rate, and the influence of the radar upgrade on service QPE was discussed. Furthermore, the error characteristics of the optimization algorithm at various distances from the radar were evaluated. Thus, the following conclusions can be drawn.

(1) Although the HCA-QPE algorithm did not use the real-time gauge-measured rainfall data for correction, its estimation accuracy was worse than that of DRVC-QPE only when the rainfall rate was smaller

than 5mm h^{-1}. As the rainfall rate increased, the accuracy of HCA-QPE became better than that of DRVC-QPE. In addition, we found that the greater the rainfall rate, the greater the improvement in estimation accuracy. Furthermore, the estimation accuracy of the HCA-QPE algorithm was better than that of the CSU-HIDRO and JPOLE algorithms.

(2) The HCA-QPE algorithm performed best in all distance ranges from the radar. The optimal performing distance range for the three optimization algorithms was 50–125 km. The estimation accuracy of the three algorithms decreased at a distance greater than 125 km, mainly due to the melting layer, loss of radar sensitivity, beam broadening and beam overshoot precipitation.

Improving the accuracy of radar QPE is a prerequisite for improving the accuracy of heavy rain forecasting. The HCA-QPE algorithm in this study is not ideal in estimating light rainfall, but is getting better in case of heavier rainfall. However, there are still many unresolved problems for HCA-QPE algorithm that requires further studies, such as the reasons why the error oscillates with increasing distance and how to improve the estimation accuracy of HCA-QPE algorithm in light rain, and so on.

REFERENCES

[1] CHANDRASEKAR V, GORGUCCI E, SCARCHILLI G. Optimization of multi-parameter radar estimates of rainfall [J]. J Appl Meteor, 1993, 32(7): 1288−1293, https://doi.org/10.1175/1520-0450(1993)032<1288:OOMREO>2.0.CO;2.

[2] GORGUCCI E, SCARCHILLI G, CHANDRASEKAR V, et al. Rainfall estimation from polarimetric radar measurements: Composite algorithms immune to variability in raindrop shape-size relation [J]. J Atmos Oceanic Technol, 2001, 18(11): 1773−1786, https://doi.org/10.1175/1520-0426(2001)018<1773:REFPRM>2.0.CO;2.

[3] RYZHKOV A V, GIANGRANDE S E, SCHUUR T J. Rainfall estimation with a polarimetric prototype of WSR-88D [J]. J Appl Meteor, 2005, 44(4): 502−515, https://doi.org/10.1175/JAM2213.1.

[4] CIFELLI R, CHANDRASEKAR V, LIM S, et al. A new dual-polarization radar rainfall algorithm: Application in Colorado precipitation events [J]. J Atmos Oceanic Technol, 2011, 28(3): 352−364, https://doi. org / 10.1175 / 2010JTECHA1488.1.

[5] RYZHKOV A V, ZRNIĆD S. Comparison of dual-polarization radar estimators of rain [J]. J Atmos Ocean Technol, 1995, 12(2): 249-256, https://doi. org / 10.1175 / 1520-0426(1995)012<0249:CODPRE>2.0.CO;2.

[6] CHEN G, ZHAO K, ZHANG G F, et al. Improving polarimetric C-band radar rainfall estimation with two-dimensional video disdrometer observations in eastern China[J]. J Hydrometeorol, 2017, 18(5): 1375-1391, https://doi.org/10.1175/JHM-D-16-0215.1.

[7] CHANDRASEKAR V, BRINGI V, BALAKRISHNAN N, et al. Error structure of multiparameter radar and surface measurements of rainfall, Part III: Specific differential phase [J]. J Atmos Oceanic Technol, 1990, 7(5): 621-629, https://doi. org / 10.1175 / 1520-0426(1990)007<0621:ESOMRA>2.0.CO;2.

[8] ZRNIĆ D, RYZHKOV A. Advantages of rain measurements using specific differential phase [J]. J Atmos Oceanic Technol, 1996, 13(2): 454-464, https://doi. org / 10.1175/1520-0426(1996)013<0454:AORMUS>2.0.CO;2.

[9] PEPLER A S, MAY P T, THURAI M. A robust error-based rain estimation method for polarimetric radar, Part I: Development of a method [J]. J Appl Meteor Climatol, 2011, 50(10): 2092-2103, https://doi.org/10.1175/JAMC-D-10-05029.1.

[10] PARK H S, RYZHKOV A V, ZRNIĆ D S, et al. The hydrometeor classification algorithm for the polarimetric WSR-88D: Description and application to an MCS [J]. Wea Forecasting, 2009, 24(3): 730-748, https://doi. org / 10.1175/2008WAF2222205.1.

[11] GIANGRANDE S E, RYZHKOV A V. Estimation of rainfall based on the results of polarimetric echo classification [J]. J Appl Meteor Climatol, 2008, 479: 2445-2462, https://doi.org/10.1175/2008JAMC1753.1.

[12] WU C, LIU L P, WEI M, et al. Statistics-based optimization of the polarimetric radar hydrometeor classification algorithm and its application for a squall line in South China [J]. Adv Atmos Sci, 2018, 35(3): 296-316, https://doi.org/ 10.1007/s00376-017-6241-0.

[13] WANG Y, FENG Y R, CAI J H, et al. An approach for radar quantitative precipitation estimate based on categorical Z-I relations [J]. J Trop Meteor, 2011, 27: 601-608 (in Chinese).

[14] WEI Q, HU Z Q, LIU L P, et al. C-band polarization radar data pre-processing and Its application to rainfall estimation [J]. Plateau Meteor, 2016, 35: 231-243 (in Chinese).

[15] WANG D, LIU L P, CHONG W. An optimization rainfall algorithm of S-Band dual-polarization radar based on hydrometeor identification [J]. Meteor Mon, 2017, 43(9): 1014-1051 (in Chinese), https://doi. org / 10.7519 / j. issn.1000-0526.2017.09.002.

[16] ZHANG Y, LIU L P, WEN H, et al. Development and assessment of quantitative precipitation estimation algorithms for S-, C-, and X-band dual-polarization radars based on disdrometer data from three regions of China [J]. J Trop Meteor, 2018, 25(2): 269-292, https://doi. org / 10.16555/j.1006-8775.2019.02.012.

[17] CHEN C, HU Z Q, HU S, et al. Preliminary analysis of data quality of Guangzhou S-band polarimetric weather Radar [J]. J Trop Meteor, 2018, 34: 59-67 (in Chinese).

[18] LIU L P, HU Z Q, FANG W G, et al. Calibration and data quality analysis with moblie C-band polarimetric radar [J]. Acta Meteor Sinica, 2010, 24: 501-509.

[19] WANG Y T, CHANDRASEKAR V. Algorithm for estimation of the specific differential phase [J]. J Atmos Oceanic Technol, 2009, 26(12): 2565-2578, https://doi. org/10.1175/2009JTECHA1358.1.

[20] ZHANG Y, LIU L P, WEN H, et al. Evaluation of the polarimetric-radar quantitative precipitation estimates of an extremely heavy rainfall event and nine common rainfall events in Guangzhou [J]. Atmos, 2018, 9(9): 330, https://doi.org/10.3390/atmos9090330.

[21] CHEN J, QIAN W M, HAN J C, et al. An approach for radar quantitative precipitation estimate based on Z-I relations varying with time and space [J]. Meteor Mon, 2015, 41(3): 296-303 (in Chinese).

[22] ZHANG P C, DAI T P, WU Z F. Principle and accuracy of

adjusting the area precipitation from digital weather radar through variational method [J]. Scientia Meteor Sinica, 1992, 16(2): 248-256.

[23] GOU Y B, LIU L P, YANG J, et al. Operational application and evaluation of the quantitative precipitation estimates algorithm based on the multi-radar mosaic [J]. Acta Meteor Sinica, 2014, 72: 731-748.

[24] RYZHKOV A V, SCHUUR T J, BURGESS D W, et al. The joint polarization experiment: polarimetric rainfall measurements and hydrometeor classification [J]. Bull Amer Meteor Soc, 2005, 86(6): 809-824, https://doi.org/10.1175/BAMS-86-6-809.

[25] SHI R, CHEN M H, CUI Z H, et al. Observational study on the real-time vertical profile of reflectivity by the Yichang's doppler radar in summer [J]. Meteor Mon, 2005, 31(9): 39-43 (in Chinese).

[26] DAI T P, FU D S, JIANG D M. Effects of the zero-layer bright-band and the atmospheric refraction on the precision of regional rainfall measured by radar [J]. J Nanjing Inst Meteor, 1991, 14: 105-112 (in Chinese).

[27] GATLIN P, PETERSEN W A, KNUPP K R, et al. Observed response of the raindrop size distribution to changes in the melting layer [J]. Atmosphere, 2018, 9(8): 319, https://doi.org/10.3390/atmos9080319.

[28] EMORY A E, DEMOZ B, VERMEESCH K, et al. Double bright band observations with high-resolution vertically pointing radar, lidar, and profilers [J]. Geophys Res Atmos, 119(13): 8201-8211, https://doi. org / 10.1002 / 2013JD020063.

Citation: CHEN Chao, LIU Li-ping, WU Zhi-fang, et al. Operational evaluation of the quantitative precipitation estimation by a CINRAD-SA dual polarization radar system[J]. J Trop Meteor, 2020, 26(2): 176-187, https://doi.org/10.46267/j.1006-8775.2020.016.

Appendix

Table 2. Rainfall events from March 1 to October 30, 2017.

No.	Date and Time (China Standard Time)	Duration (h)	Precipitation Type
1	07:00 March 7 to 12:00 March 8	29	Stratus
2	05:00 March 9 to 20:00 March 10	39	Stratus
3	04:00 March 11 to 11:00 March 12	31	Stratus
4	01:00 March 18 to 23:00 March 19	46	Stratocumulus
5	00:00 to 21:00 March 22	21	Stratus
6	21:00 March 28 to 13:00 March 29	14	Stratocumulus
7	00:00 March 31 to 01:00 April 1	25	Stratocumulus
8	08:00 to 23:00 April 11	15	Stratocumulus
9	16:00 to 23:00 April 12	7	Stratocumulus
10	10:00 April 19 to 02:00 April 20	16	Stratocumulus
11	10:00 April 20 to 20:00 April 21	34	Stratocumulus
12	08:00 April 22 to 23:00 April 23	39	Stratus
13	20:00 April 24 to 07:00 April 27	59	Stratocumulus
14	18:00 to 23:00 May 2	5	Convective Clouds
15	04:00 to 11:00 May 4	7	Stratocumulus
16	00:00 to 20:00 May 7	20	Stratocumulus
17	16:00 to 23:00 May 8	7	Stratocumulus
18	07:00 to 12:00 May 12	5	Convective Clouds
19	17:00 May 14 to 06:00 May 16	37	Stratocumulus
20	15:00 to 21:00 May 21	6	Stratocumulus
21	18:00 to 23:00 May 23	5	Convective Clouds
22	06:00 to 13:00 May 24	7	Stratocumulus
23	09:00 to 15:00 June 9	6	Stratocumulus
24	02:00 to 13:00 June 14	11	Stratocumulus
25	18:00 June 15 to 13:00 June 18	65	Stratocumulus
26	12:00 to 17:00 June 19	5	Convective Clouds
27	10:00 to 22:00 June 20	12	Stratocumulus
28	13:00 to 22:00 June 21	9	Stratocumulus
29	12:00 to 19:00 June 23	7	Stratocumulus
30	00:00 July 2 to 16:00 July 4	64	Stratocumulus
31	12:00 to 18:00 July 5	6	Convective Clouds
32	10:00 to 18:00 July 6	8	Convective Clouds
33	12:00 to 20:00 July 8	8	Convective Clouds
34	12:00 to 17:00 July 10	5	Convective Clouds
35	08:00 to 18:00 July 11	10	Convective Clouds
36	13:00 to 21:00 July 13	8	Convective Clouds
37	14:00 July 15 to 03:00 July 19	85	Stratocumulus
38	10:00 to 20:00 July 19	10	Stratocumulus
39	13:00 to 20:00 July 21	7	Convective Clouds
40	00:00 July 23 to 01:00 July 24	25	Stratocumulus
41	17:00 August 1 to 17:00 August 2	24	Convective Clouds
42	09:00 to 19:00 August 3	10	Convective Clouds
43	10:00 to 15:00 August 11	5	Convective Clouds
44	13:00 August 22 to 22:00 August 24	57	Stratocumulus
45	17:00 August 26 to 19:00 August 28	50	Stratocumulus
46	05:00 to 23:00 September 4	18	Stratocumulus
47	11:00 September 5 to 00:00 September 6	13	Convective Clouds
48	08:00 to 17:00 September 7	9	Convective Clouds
49	14:00 to 19:00 September 21	5	Convective Clouds
50	13:00 to 18:00 September 29	5	Convective Clouds
51	17:00 October 15 to 20:00 October 16	27	Stratocumulus